

FIELD–GUIDED PROTON ACCELERATION AT RECONNECTING X–POINTS IN FLARES

B. Hamilton¹, K. G. McClements², L. Fletcher¹, A. Thyagaraja²

¹Department of Physics and Astronomy, University of Glasgow, Glasgow, G12 8QQ, UK

²UKAEA Culham Division, Culham Science Centre, Abingdon, Oxfordshire, OX14 3BD, UK

Abstract

An explicitly energy–conserving full orbit code CUEBIT, developed originally to describe energetic particle effects in laboratory fusion experiments, has been applied to the problem of proton acceleration in solar flares. The model fields are obtained from solutions of the linearised MHD equations for reconnecting modes at an X–type neutral point, with the additional ingredient of a longitudinal magnetic field component. To accelerate protons to the highest observed energies on flare timescales, it is necessary to invoke anomalous resistivity in the MHD solution. It is shown that the addition of a longitudinal field component greatly increases the efficiency of ion acceleration, essentially because it greatly reduces the magnitude of drift motions away from the vicinity of the X–point, where the accelerating component of the electric field is largest. Using plasma parameters consistent with flare observations, we obtain proton distributions extending up to γ –ray–emitting energies (> 1 MeV). In some cases the energy distributions exhibit a bump–on–tail in the MeV range. In general, the shape of the distribution is sensitive to the model parameters.

Accepted for publication in *Solar Physics* February 20 2003

1 Introduction

The process of magnetic reconnection is believed to be intrinsic to solar flares. It is invoked as the mechanism whereby energy-loaded magnetic fields can reconfigure to a lower energy state, liberating the energy which powers particle acceleration, heating, and mass motions. As the resistivity of solar coronal material is very low, the large reconnection rate required to power a flare demands the presence of reconnecting structures with very small length scales – namely, current sheets. Both in solar and magnetospheric physics, the study of particle acceleration in such structures has received considerable attention over the past few decades. Under non-steady state conditions, a reconnecting magnetic field produces an inductive electric field \mathbf{E} : the resistive magnetohydrodynamic (MHD) form of Ohm’s law indicates that in general this \mathbf{E} has a component parallel to the local magnetic field, and can thus accelerate charged

particles. An example of such a non-steady state is a perturbed reconnecting X-type neutral point, for which Craig and McClymont (1991) calculated the normal modes in a strictly 2-D field, $\mathbf{B}(x, y)$. In this paper we demonstrate that the analysis of Craig and McClymont is applicable when a z -invariant component of the magnetic field is included, enabling it to be extended to configurations more likely to be representative of conditions in the flaring solar corona.

In the context of solar flare physics, a current sheet is often envisaged as arising in a two-ribbon flare, where reconnection of oppositely-directed, predominantly vertical magnetic fields results in a sheet structure having a length (parallel to the solar surface) on the order of the length of a post-flare arcade ($\sim 10^7\text{m}$), a vertical extent (height perpendicular to the solar surface) comparable to this, and a thickness on the order of a few times the ion gyroradius. Particle acceleration - in particular proton acceleration - in just such a (collisionless) reconnecting current sheet was addressed by Martens (1998). Following from the magnetotail work of Speiser (1965) he considered the effects of the inclusion of a component of magnetic field perpendicular to the plane of the current sheet, deriving expressions for the maximum energy attained before the gyromotion around this perpendicular field causes the protons to exit the sheet, and hence the acceleration region. With reconnection electric field strengths comparable with those observed (e.g. Kopp and Poletto, 1986), it was found that the proton energy and flux budgets for flares were compatible with those arising from acceleration in a macroscopic current sheet (for example formed in the wake of a rising filament, with vertical extent on the order of 10^7m , comparable to its length).

Litvinenko and Somov (1993) also considered the current sheet geometry, demonstrating the effects of the addition of a further magnetic field component parallel to the direction of the reconnection electric field. A component of the charged particles' motion is then gyration about this parallel field, which allows them to stay longer in the current sheet, and attain higher energies. It is this fact which also becomes important in our studies.

While a reconnecting current sheet with finite (and large) vertical extent is frequently used in considering acceleration in large two-ribbon flares, where such a configuration is expected on the basis of numerical simulations of filament lift-off, we concern ourselves here with a current sheet of zero vertical extent, i.e. a coronal X-line, which corresponds to the initial stages of reconnection behind a filament. In the simplest case, this configuration is identical in cross-section [the (x, y) plane] to a 2-D X-type neutral point, but is invariant in the z -direction. In reality, true magnetic nulls ($B \rightarrow 0$) are likely to be rare in the corona. The elaboration of this scenario which we study here, and find to have important consequences for particle acceleration, is the inclusion of a component of magnetic field also in the z -direction.

Proton acceleration at an X-point with finite B_z was investigated by Bulanov (1980), Mori, Sakai, and Zhao (1998), Browning and Vekstein (2001), and Bruhwiler and Zweibel (1992). The present study differs from that of previous workers in that the accelerating electric field E_z is obtained self-consistently from a magnetic flux function corresponding to a reconnecting eigenmode of the X-point. This perturbation solution

was invoked in the context of particle acceleration also by Petkaki and MacKinnon (1997), but without the addition of the finite B_z component.

A major challenge for any flare acceleration mechanism is to obtain sufficient high energy particles in a short timescale; new observations from the RHESSI satellite are putting ever tighter constraints on timescales, spectra and total energies. The typical requirements for protons, as summarised by Miller (1998) are as follows: they are accelerated up to energies of ~ 100 MeV on timescales of about a second, and to about a GeV on timescales of a few seconds. Proton acceleration lasts for several tens of seconds, at a rate of $\sim 10^{35}\text{s}^{-1}$, such that the total energy content in protons above an MeV is $\sim 10^{24}$ J. Given a coronal density of $10^{15} - 10^{16}\text{m}^{-3}$ and volume of $\sim 10^{21}\text{m}^{-3}$, this implies that each second around 1-10% of all coronal protons must be accelerated to MeV energies (and therefore require rapid replenishing - we do not address this here). We find that the inclusion of a moderate longitudinal field component greatly assists in this process.

This paper is structured in the following way. In Section 2 we describe our new algorithm for particle calculations. Section 3 describes the model employed in the simulations. Some sample simulation results and the effect of varying parameters of the simulation, such as the strength of the z component of the magnetic field, are described in Section 4 and we end with discussions and conclusions in Section 5.

2 Energy–Conserving Algorithm

The nonrelativistic Lorentz force equations

$$m\frac{d\mathbf{v}}{dt} = Ze\mathbf{v} \times \mathbf{B}(\mathbf{x}) + Ze\mathbf{E}(\mathbf{x}), \quad \frac{d\mathbf{x}}{dt} = \mathbf{v}, \quad (1)$$

are approximated in the CUEBIT (CULham Energy–conserving orBIT) code by the following finite difference equations

$$m\frac{\mathbf{v}^{i+1} - \mathbf{v}^i}{\Delta t} = Ze\left(\frac{\mathbf{v}^{i+1} + \mathbf{v}^i}{2}\right) \times \mathbf{B}\left(\frac{\mathbf{x}^{i+1} + \mathbf{x}^i}{2}\right) + Ze\mathbf{E}\left(\frac{\mathbf{x}^{i+1} + \mathbf{x}^i}{2}\right), \quad (2)$$

$$\frac{\mathbf{x}^{i+1} - \mathbf{x}^i}{\Delta t} = \frac{\mathbf{v}^{i+1} + \mathbf{v}^i}{2}. \quad (3)$$

Here m , Ze denote particle mass and charge. At the start of each timestep \mathbf{x}^{i+1} is set equal to \mathbf{x}^i in a first calculation of \mathbf{v}^{i+1} . A few iterations are made which converge quickly to a final \mathbf{v}^{i+1} .

Mori, Sakai and Zhao (1998) also used a scheme in which \mathbf{v} was set equal to $(\mathbf{v}^{i+1} + \mathbf{v}^i)/2$ on the right hand side of the Lorentz force equation. In the special case where $\mathbf{E} = 0$, the scalar product of the right hand side of Equation (2) with $\mathbf{v}^{i+1} + \mathbf{v}^i$ is identically zero, so that $(v^{i+1})^2 = (v^i)^2$. The scheme thus conserves energy exactly. This makes it possible to obtain accurate results with relatively long timesteps. A modified version of Equation (2) conserves total energy exactly when

\mathbf{E} is a finite potential electric field. For non-potential electric fields, such as those arising from magnetic reconnection, we have found the method remains accurate for large timesteps (exceeding the Larmor period in most of the computational domain), allowing large numbers of particles to be simulated for timescales that are relevant for flare acceleration. CUEBIT has also been benchmarked by using it to compute energetic particle orbits in magnetic fusion experiments (Wilson et al., 2002), and will in the future be used to study particle transport under various conditions (e.g. in the presence of turbulent electromagnetic fields) in such experiments.

For the simulations discussed in Section 4 it is not necessary to incorporate relativistic kinematics in Equation (2) as the energies reached are only a small fraction of the particles' rest mass energy (we consider only proton acceleration). However, a relativistic version of the code is currently being developed for the purpose of describing electron acceleration and transport.

3 Model of a reconnecting X-type structure

3.1 Craig and McClymont solution

For a simple model of a reconnecting field at an X-type neutral point we use the two-dimensional description of Craig and McClymont (1991), with the additional element of a finite third magnetic field component B_z . To determine the conditions under which the Craig and McClymont analysis applies with $B_z \neq 0$, we re-derive below their equations for the evolution of a flux function ψ , defined such that the curl of $\mathbf{A} \equiv \psi \hat{\mathbf{z}}$ is equal to the magnetic field in the (x, y) plane. The induction equation

$$\frac{\partial \mathbf{B}}{\partial t} = \nabla \times (\mathbf{v} \times \mathbf{B}) + \frac{\eta}{\mu_0} \nabla^2 \mathbf{B}, \quad (4)$$

can be written in the form

$$\frac{\partial \mathbf{A}}{\partial t} = \mathbf{v} \times (\nabla \times \mathbf{A}) + \frac{\eta}{\mu_0} \nabla^2 \mathbf{A}. \quad (5)$$

Here \mathbf{v} is flow velocity, η is resistivity (assumed to be constant) and μ_0 is the permeability of free space. The first term on the right hand side of Equation (5) can be expanded to give

$$\mathbf{v} \times (\nabla \times \mathbf{A}) = \nabla (\mathbf{v} \cdot \mathbf{A}) - (\mathbf{v} \cdot \nabla) \mathbf{A} - \mathbf{A} \times (\nabla \times \mathbf{v}) - (\mathbf{A} \cdot \nabla) \mathbf{v}. \quad (6)$$

We assume that flows only occur in the (x, y) plane and that there are no variations in the z -direction. In these circumstances the first, third and fourth terms on the right hand side of Equation (6) are all zero and Equation (5) reduces to

$$\frac{\partial \psi}{\partial t} + (\mathbf{v} \cdot \nabla) \psi = \frac{\eta}{\mu_0} \nabla^2 \psi, \quad (7)$$

which is the form of the induction equation used by Craig and McClymont.

Neglecting plasma pressure, viscosity and any external forces such as gravity the momentum equation is

$$\frac{\partial \mathbf{v}}{\partial t} + (\mathbf{v} \cdot \nabla) \mathbf{v} = \frac{1}{\rho} \mathbf{j} \times \mathbf{B}, \quad (8)$$

where \mathbf{j} , ρ denote current and mass density. Now in the present case

$$\mathbf{j} = \frac{1}{\mu_0} \nabla \times \mathbf{B} = -\frac{\hat{\mathbf{z}}}{\mu_0} \nabla^2 \psi. \quad (9)$$

Substituting this expression into Equation (8) and noting that $\nabla \psi$ is in the (x, y) plane, we obtain

$$\frac{\partial \mathbf{v}}{\partial t} + (\mathbf{v} \cdot \nabla) \mathbf{v} = -\frac{1}{\mu_0 \rho} (\nabla^2 \psi) \nabla \psi, \quad (10)$$

i.e. Equation (2.3) in Craig and MyClymont (1991).

3.2 Extension of Craig and McClymont solution to $B_z \neq 0$

We now assume that the \mathbf{B} field is of the form

$$\mathbf{B} = \nabla \times (\psi \hat{\mathbf{z}}) + B_z \hat{\mathbf{z}}, \quad (11)$$

where B_z is constant and uniform. As before, we assume that there are no variations in the z direction. Substituting Equation (11) into Equation (4) and writing $\mathbf{A} = \psi \hat{\mathbf{z}}$ as before gives

$$\frac{\partial}{\partial t} (\nabla \times \mathbf{A} + B_z \hat{\mathbf{z}}) = \nabla \times (\mathbf{v} \times (\nabla \times \mathbf{A} + B_z \hat{\mathbf{z}})) + \frac{\eta}{\mu_0} \nabla^2 (\nabla \times \mathbf{A} + B_z \hat{\mathbf{z}}). \quad (12)$$

Since B_z is constant and uniform this reduces to

$$\frac{\partial}{\partial t} (\nabla \times \mathbf{A}) = \nabla \times (\mathbf{v} \times (\nabla \times \mathbf{A})) + \nabla \times [\mathbf{v} \times (B_z \hat{\mathbf{z}})] + \frac{\eta}{\mu_0} \nabla^2 (\nabla \times \mathbf{A}). \quad (13)$$

This is equivalent to the induction equation of Craig and McClymont except for the term containing B_z on the right hand side. This term can be written in the form

$$\nabla \times [\mathbf{v} \times (B_z \hat{\mathbf{z}})] = - (B_z \hat{\mathbf{z}}) \nabla \cdot \mathbf{v}. \quad (14)$$

Since B_z is not necessarily zero, the only way for this quantity to be zero is if $\nabla \cdot \mathbf{v} = 0$, i.e. the plasma flow must be incompressible. This assumption is often invoked in studies of magnetic reconnection (e.g. Biskamp, 2000; Priest and Forbes, 2001), and is a reasonable one for solar flare plasmas. Incompressibility is implicit in the model of Craig and McClymont: they use Equation (10) in a dimensionless form that is only valid if the plasma density is constrained to be uniform and time-independent. In the limit of ideal MHD, it is straightforward to show that the flow must be incompressible

when, as in the scenario considered here, there are no variations in the z -direction and B_z is finite (Strauss, 1976). With the assumption of incompressibility, Equation (7) is valid for finite B_z . Moreover, since B_z is curl-free it does not contribute to the current; since the latter is oriented in the z direction [Equation (9)], it follows that B_z does not contribute to the Lorentz force either, and thus the momentum equation of Craig and McClymont [Equation (10)] also remains valid. The solutions of these equations derived by Craig and McClymont are therefore applicable when the magnetic field has a uniform and static z component.

3.3 Perturbation solution

The equilibrium X-type neutral point structure invoked by Craig and McClymont (1991) is described by

$$\mathbf{B} = \frac{B_o}{R_o} (y\hat{\mathbf{x}} + x\hat{\mathbf{y}}), \quad (15)$$

where B_o is the field strength at the (circular) boundary of the system where $R = R_o$, R being the radial co-ordinate measured from the z -axis outwards. Perturbations to this field geometry will result in normal modes of oscillation. Following Petkaki and MacKinnon (1997), we consider only the fundamental mode, with zero azimuthal and radial mode numbers. Approximate analytical solutions for the perturbed magnetic and electric fields can be obtained by dividing the system into an ideal outer region and a resistive inner region, separated by a critical radius

$$R_c = R_o \left(\frac{2}{S} \right)^{\frac{1}{2}}, \quad (16)$$

where S , the Lundquist number at the boundary $R = R_o$, is equal to $\mu_0 R_o v_A / \eta$ where v_A is the Alfvén speed at $R = R_o$. The solution for the perturbed magnetic field in cylindrical polar coordinates can be approximated by (Craig and McClymont, 1991)

$$\delta B = -dB \frac{R_o}{R} \omega \cos \left(\omega \ln \frac{R}{R_o} \right) \cos \left(\frac{\omega v_A t}{R_o} \right) \exp \left(-\frac{\alpha v_A t}{R_o} \right) \hat{\phi}, \quad (17)$$

for $R > R_c$. Here dB is an arbitrary scaling parameter, ω is a dimensionless mode frequency, α is a dimensionless decay constant and $\hat{\phi}$ is the unit vector in the azimuthal direction. For $R \leq R_c$ the magnetic field perturbation is zero. The value of ω is determined by the requirement that Equation (17) yields $\delta B = 0$ at $R = R_c$, and $\alpha \simeq \omega^2/2$ (Craig and McClymont, 1991). The electric field resulting from this solution is wholly in the z -direction and is given by

$$E_z = dB v_A \sin \left(\omega \ln \frac{R}{R_o} \right) \exp \left(-\frac{\alpha v_A t}{R_o} \right) \left(\alpha \cos \left(\frac{\omega v_A t}{R_o} \right) + \omega \sin \left(\frac{\omega v_A t}{R_o} \right) \right), \quad (18)$$

for $R > R_c$ and

$$E_z = -dB v_A \exp \left(-\frac{\alpha v_A t}{R_o} \right) \left(\alpha \cos \left(\frac{\omega v_A t}{R_o} \right) + \omega \sin \left(\frac{\omega v_A t}{R_o} \right) \right), \quad (19)$$

for $R \leq R_c$. Equations (17), (18), and (19) remain valid for an incompressible plasma with finite B_z constant in time and space. We show below that the inclusion of a modest B_z dramatically increases the efficiency with which test particles are accelerated in this magnetic geometry.

4 Acceleration in a reconnecting X-type structure

4.1 Choice of parameters

We consider specifically the acceleration of test particle protons in a prescribed field of the type discussed in the previous section. It is known that protons are accelerated in flares to energies of at least several tens of MeV in a timescale of the order of one second (Miller, 1998; Aschwanden, 2002). A straightforward calculation indicates that this could be achieved with a parallel electric field E_{\parallel} of around 1 Vm^{-1} . Such field strengths are, incidentally, consistent with the parallel electric fields implied by observations of the separation rates of flare ribbons, e.g. Kopp and Poletto (1986). However, as noted recently by Craig and Litvinenko (2002), fields of this magnitude are not consistent with classical Spitzer resistivity. In deriving their reconnecting field solutions, Craig and McClymont (1991) used the resistive MHD form of Ohm's law, i.e. $E_{\parallel} = \eta j_{\parallel}$ where j_{\parallel} is the parallel component of \mathbf{j} . The maximum possible current density in a hydrogen plasma is $j_{\max} = 2nec$, where n is particle density and c is the speed of light. So a coronal density of $10^{15} - 10^{16} \text{ m}^{-3}$ implies that $j_{\max} \sim 10^5 - 10^6 \text{ Am}^{-2}$. However, if the resistivity were determined by classical electron-ion collisions, and the plasma temperature T were equal to 10^7 K , a field of 1 Vm^{-1} would produce a steady-state current density of around $2 \times 10^7 \text{ Am}^{-2}$. This high current cannot be sustained by a classical collisional resistivity. We deduce that protons can only be accelerated to γ -ray-emitting energies in a reconnecting field of the type invoked by Craig and McClymont if η is much higher than the Spitzer value, i.e. it is anomalous. Craig and Litvinenko (2002) have pointed out another reason for ruling out Spitzer resistivity in the flaring corona, namely that it implies a resistive scale length that is smaller than the collisional mean free path.

Anomalous resistivity can result from lower hybrid or ion acoustic micro-turbulence. Whether lower hybrid or ion acoustic waves are more likely to produce the required anomalous resistivity depends on several parameters, including the ratio of plasma pressure to magnetic field pressure, the electron to ion temperature ratio, and the direction of the current relative to the local magnetic field (Aparicio et al., 1998; Biskamp, 2000). In either case, turbulence results from the current density exceeding a certain threshold κnec_s where c_s is the sound speed and κ is a numerical factor typically ranging from unity up to about the square root of the ion to electron mass ratio (Kulsrud, 1998; Aparicio, *et al.* 1998). The anomalous resistivity then prevents the current density from exceeding this threshold: the turbulence increases the effective collisionality of the plasma. In the case of ion acoustic turbulence, for example, there is a strong interaction with protons whose velocity component v parallel to the wave propagation

direction is of the order of c_s (Ishihara and Hirose, 1981). The strength of the interaction falls off roughly as $1/v^2$, and is negligibly small for particles lying sufficiently far out in the tail of a Maxwellian distribution (cf. Litvinenko and Somov, 1993). Therefore, some small fraction of the initial proton population is effectively collisionless, and can be described using Equation (1): it is this sub-population of protons which we simulate using CUEBIT. The bulk of the plasma is effectively collisional, due to the anomalous resistivity. The use of a test particle approach requires that any net current associated with accelerated particles is small compared to the current corresponding to the reconnecting field.

For simplicity, the particles in most of our simulations were given zero initial velocity. This is permissible, since the thermal spread of velocities corresponding to a typical coronal temperature is very small compared to the near-relativistic speeds required for protons to excite γ -ray emission, and we will show that the final proton energy spectrum above ~ 10 keV in a typical simulation does not change significantly when the δ -function initial velocity distribution is replaced with a 10^7 K Maxwellian.

The choice of parameters in the simulations is dictated in part by the limits imposed by anomalous resistivity, combined with the typical parallel field strengths needed. We assume, for definiteness $n = 10^{16} \text{m}^{-3}$, $R_o = 10^7 \text{m}$ and $B_o = 0.01 \text{T}$. If the temperature is assumed to be 10^7K , and the current is assumed to be limited to nec_s (i.e. $\kappa = 1$), the anomalous resistivity required for $E_{\parallel} = 1 \text{Vm}^{-1}$ is then $1.4 \times 10^{-3} \Omega \text{m}$ and the Lundquist number at the boundary $R = R_o$ (a key parameter in the Craig and McClymont model) is $S \simeq 2 \times 10^{10}$. Equations (3.6) and (3.8) of Craig and McClymont (1991) then yield $\omega \simeq 0.13$ and $\alpha \simeq 0.0088$. The scaling parameter dB in Equations (17), (18) and (19) was chosen to give $E_z \simeq 1 \text{Vm}^{-1}$ at $t = 0$ and $R < R_c$ (in this region $E_z \simeq E_{\parallel}$) rising to approximately 1.4Vm^{-1} after 1 s. For comparison, simulations were also carried out with $E_z = 0.1 \text{Vm}^{-1}$ and 10Vm^{-1} . Strictly speaking, a change in E_z implies a change in η and hence S if the limiting current is assumed to be a fixed multiple of nec_s . However, since ω and α have only a weak (logarithmic) dependence on S , the same values of these parameters were used in all the simulations.

The only remaining parameter to fix is B_z . It follows from the conclusions drawn in Section 3.2 that this can be varied freely without any of the other parameters being affected. Simulations were carried out with $B_z = 0 \text{T}$, 10^{-5}T , 10^{-4}T , 10^{-3}T and 10^{-2}T : these are all reasonable values for active region coronal magnetic fields.

4.2 Results

In each simulation the trajectories were computed of approximately 10^6 protons with an initially uniform random distribution of positions in the reconnection region ($R \leq R_o$), and, unless otherwise stated, a δ -function velocity distribution. The duration of each simulation, 1 s, was chosen on the basis that protons appear to be accelerated to tens of MeV on timescales of this order (Miller, 1998; Aschwanden, 2002). The timestep Δt was of the order of 100 Larmor periods calculated at $R = R_o$ (simulations with shorter timesteps produced essentially identical results); there were approximately 1500

timesteps per simulation. The value of dB was chosen such that the magnitude of the magnetic field perturbation at $R = R_o$ and $t = 0$ was always $\leq 10^{-4}$ T.

Figure 1 shows R and particle energy E as functions of time for a proton initially lying close to the X-point ($R = 10\text{m}$) in field configurations with $B_z = 0$ (solid curves) and $B_z = 10^{-4}$ T (dashed curves). The other field parameters are those listed at the end of the previous section. The proton initially lies at azimuthal angle $\varphi = 24^\circ$ in the (x, y) plane, and has velocity components in the cylindrical coordinate system $v_R = v_\varphi = v_z = 10^5 \text{ms}^{-1}$.

It is immediately clear that the addition of even a very modest B_z has a dramatic effect on the trajectory of the particle in phase space. When $B_z = 0$ the total magnetic field is very small close to the X-point (since $\delta B = 0$ in this region). The Lorentz force in the (x, y) plane is consequently very weak, the particle is effectively unmagnetised, and hence moves rapidly away from the X-point. There is only a short phase of acceleration (in this case to about 1 keV): far from the X-point, the particle becomes magnetized and, since \mathbf{B} is strictly perpendicular to \mathbf{E} , there is no further acceleration. However, a longitudinal field of 10^{-4}T is sufficient to confine the particle to within a few tens of metres of the X-point, with the result that acceleration to energies of 100 keV and above can easily occur. Because B_z is assumed to be uniform and the field components in the (x, y) plane are very small, the combined effect of $\text{grad}B$, curvature and $\mathbf{E} \times \mathbf{B}$ drifts on the particle trajectory is negligible.

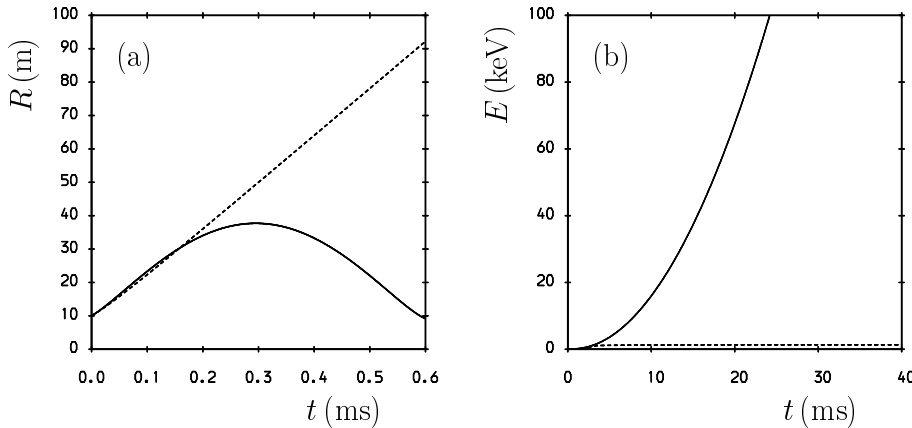


Fig. 1. Distance from the X-point versus time for particles initially lying close to $R = 0$ in field configurations with $B_z = 0$ (solid curve) and $B_z = 10^{-4}$ T (dashed curve). (b) Energy versus time over a longer timescale for the particles whose drifts are shown in (a).

Figure 2 shows final proton energy spectra for $B_z = 10^{-4}\text{T}$ and initial electric field in the inner resistive region $E_{0z} = 1\text{Vm}^{-1}$. Two different initial proton distributions were used: a δ -function (faint curve) and a 10^7K Maxwellian (bold curve). In both cases, protons are accelerated to energies of up to several MeV. The only significant

differences between the two distributions occur at energies < 10 keV: above this energy, the final distribution is insensitive to the initial conditions.

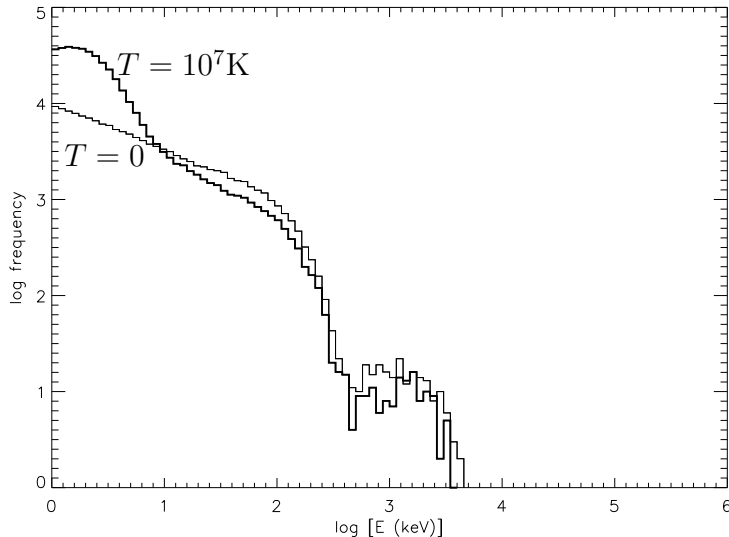


Fig. 2. Final proton energy distributions for $B_z = 10^{-4}$ T, $E_{0z} = 1$ Vm $^{-1}$. The initial distributions have temperature $T = 0$ (faint curve) and $T = 10^7$ K (bold curve).

Figures 3 and 4 show final proton energy distributions for several pairs of values of B_z and E_{0z} . In every case a δ -function initial distribution was used. In Figure 3 $B_z = 10^{-4}$ T and E_{0z} ranges from 0.1 Vm $^{-1}$ to 10 Vm $^{-1}$. Not surprisingly, protons are accelerated to higher energies as E_{0z} is increased. In contrast to the results obtained by Mori, Sakai, and Zhao (1998), the shape of the accelerated proton spectrum depends strongly on the model parameters: although in some cases the protons have a power law spectrum at low energy (1–100 keV for $E_{0z} = 1$ Vm $^{-1}$), the power law index varies considerably. It should be noted that the frequencies f plotted in Figures 3 and 4 represent the number of particles at the end of each simulation with energies in a fixed range of values of $\log_{10} E$, i.e.

$$f(E)d(\log_{10} E) \propto F(E)dE, \quad (20)$$

where F is the true energy distribution. Thus, $F(E) \propto f(E)/E$. At low energy, the distributions in Figure 3 correspond to $F(E) \propto E^{-\gamma}$ where $\gamma \leq 2$: Mori, Sakai, and Zhao (1998) obtained $\gamma \simeq 2.0 - 2.2$.

Another striking feature of the distributions in Figure 3 is the formation of a bump-on-tail at high energy. This also occurs in the simulations of Petkaki and MacKinnon (1997), but not in those of Mori, Sakai and Zhao (1998). In general, models in which there is preferential acceleration of a small sub-population of protons to MeV energies

and above are more efficient than models which predict monotonic decreasing spectra, since it is only at high energy that direct observational evidence for accelerated protons exists. The occurrence of bumps-on-tail in our simulations and those of Petkaki and MacKinnon, and their absence from those of Mori, Sakai and Zhao (1998), appears to be due to the choice of field configuration used in these studies. Mori and co-workers assumed a purely hyperbolic magnetic field in the (x, y) plane (i.e. $\delta B = 0$) and a uniform E_z . With finite B_z , there is then a large parallel electric field component $E_{\parallel} = E_z B_z / B^2$ throughout the computational domain, and all the test particles are susceptible to strong acceleration. In our case, E_{\parallel} is significantly reduced outside the critical radius $R = R_c$, due to the presence of a perturbation to the hyperbolic magnetic field ($\delta B \neq 0$) and also a fall-off in E_z associated with the spatial profile of the reconnecting mode eigenfunction [cf. Equation (18)]. Consequently, particles initially lying inside $R = R_c$ are subject to stronger acceleration than those initially lying outside.

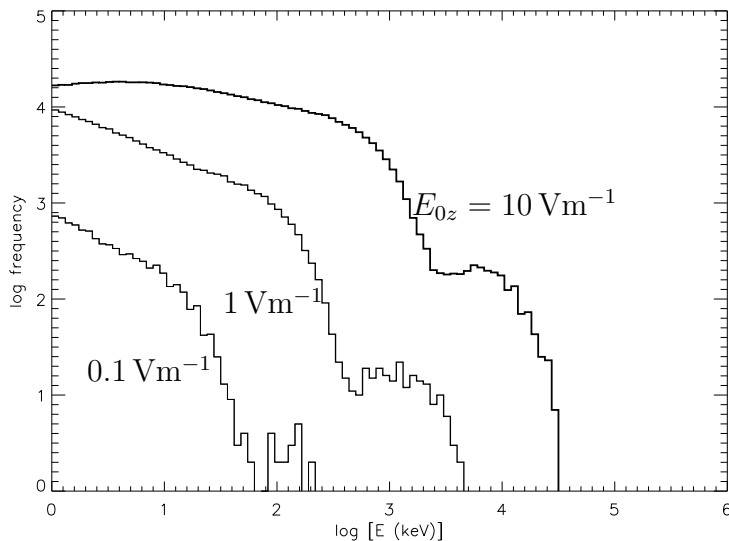


Fig. 3. Final proton energy distributions for $B_z = 10^{-4}$ T and three values of E_{0z} .

Final proton distributions are shown in Figure 4 for $E_{0z} = 1$ Vm $^{-1}$ and four different values of B_z . Results are not shown for $B_z = 0$ since in this case the number of particles accelerated to energies of more than 1 keV was negligible. It can be seen that protons are accelerated to progressively higher energies as B_z is increased – in the case of $B_z = 10^{-2}$ T, particle energies of up to 40 MeV are observed. This appears to be due simply to improved particle confinement close to the X-point: the amplitude of the sinusoidal variation in Figure 1(a) varies as $1/B_z$ and the drift speed varies as $1/B_z^2$. For $B_z < 10^{-2}$ T bump-on-tail formation at high energy is again apparent.

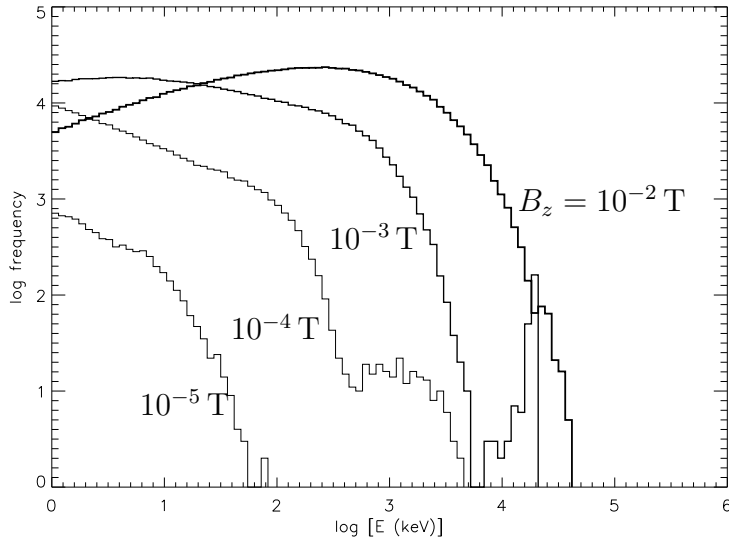


Fig. 4. Final proton energy distributions for $E_{0z} = 1 \text{ Vm}^{-1}$ and four values of B_z .

5 Discussion and Conclusions

The addition of a longitudinal field component to a two-dimensional reconnecting magnetic configuration massively increases the efficiency of particle acceleration in such configurations. Physically, this is due to the fact that particles close to the magnetic X-point are strongly magnetized by the longitudinal field and are not subject to strong $\text{grad-}B$, curvature or $\mathbf{E} \times \mathbf{B}$ drifts. The effect of a small but finite longitudinal field B_z on particle acceleration is so dramatic that $B_z = 0$ should be regarded as a singular case, unlikely to be representative of the conditions prevailing in the flaring corona. MeV protons can still be produced when $B_z = 0$, but the number of particles accelerated to such energies is only significant if the resistivity η is assumed to be extremely large – much larger even than the anomalous values corresponding to ion acoustic or lower hybrid turbulence (Petkaki and MacKinnon, 1997). A key result of the present study is that the presence of a longitudinal guide field makes it possible for protons to reach MeV energies in a plasma with realistic values of η .

In the case of the simulation with $B_z = 10^{-2} \text{ T}$, $E_{0z} = 1 \text{ Vm}^{-1}$, 14% of the protons reach energies exceeding 1 MeV in 1s. However, as discussed in Section 4.1, only a fraction of the initial particle population is modelled using the collisionless equations of motion, and so the simulation results imply a super-MeV proton fraction of much less than 14%. As noted in Section 1, observations imply that up to 1-10% of the protons in the flaring corona are accelerated per second. While the test particle method adopted here yields valuable insights into the physics of proton acceleration in flares, a more

self-consistent approach may be required to meet the tight constraints on energetic proton fluxes imposed by recent observations.

The sensitivity of the final distributions to B_z (Figure 4) suggests that it might be possible to set constraints on the value of this parameter using γ -ray observations. However, it is not clear to what extent the simulation results depend on other features of the model, such as the assumption of an azimuthally-symmetric, centrally-peaked perturbation to the magnetic flux. CUEBIT could be used to study particle acceleration in X-point field configurations with a range of different normal mode perturbations. We also intend to study electron acceleration: the numerical scheme in Equations (2) and (3) allows sufficiently large timesteps (relative to the Larmor period) to make this feasible, although it will probably be essential to use a fully relativistic version of the code in this case. Collisions can also be added to the scheme in a straightforward way, enabling simulations to be carried out on longer timescales.

In analytical studies of particle acceleration at reconnecting current sheets Litvinenko and Somov (1993) and Litvinenko (1996) formulated expressions for critical values of B_z , such that particles are efficiently accelerated, and for the typical energies which they can reach. Our results are not directly comparable to those of Litvinenko and Somov, since we have invoked a different field configuration. However, our particle code could be applied to the particular current sheet geometry invoked by these authors and their analytical results compared with simulations.

Acknowledgements

The authors are grateful to Gordon Emslie and Alec MacKinnon for helpful discussions. BH was supported by an EPSRC CASE studentship, and the work was also funded partly by the UK Department of Trade and Industry.

References

- Aparicio, J., Haines, M.G., Hastie, R.J., and Wainwright, J.P.: 1998, *Phys. Plasmas* **5**, 3180.
- Aschwanden, M.J.: 2002, *Space Science Reviews* **101**, 1.
- Biskamp, D.: 2000, *Magnetic Reconnection in Plasmas*, Cambridge University Press, Cambridge, p. 36.
- Browning, P.K. and Vekstein, G.E.: 2001: *J. Geophys. Res.* **106**, 18677.
- Bruhwyler, D.L. and Zweibel, E.G.: 1992, *J. Geophys. Res.* **97**, 10825.
- Bulanov, S.V.: 1980, *Sov. Astron. Lett.* **6**, 206.
- Craig, I.J.D. and Litvinenko, Yu.E.: 2002, *Astrophys. J.* **570**, 387.
- Craig, I.J.D. and McClymont A.N.: 1991, *Astrophys. J.* **371**, L41.
- Ishihara, O. and Hirose, A.: 1981, *Phys. Rev. Lett.* **46**, 771.
- Kopp, R. A. and Poletto, G.: 1986, in A. Poland (ed.), *Coronal and Prominence Plasmas*, NASA CP 2442, p. 469.

- Kulsrud, R.M.: 1998, *Phys. Plasmas* **5**, 1599.
- Litvinenko, Y.E.: 1996, *Astrophys. J.* **462**, 997.
- Litvinenko, Y.E. and Somov, B.V.: 1993, *Solar Phys.* **146**, 127.
- Martens, P.C.H.: 1988, *Astrophys. J.* **330**, L131.
- Miller, J. A.: 1998, *Space Science Reviews* **86**, 79.
- Mori, K., Sakai, J., and Zhao, J.: 1998, *ApJ* **494**, 430.
- Petkaki, P. and MacKinnon, A.L.: 1997, *Solar Phys.* **172**, 279.
- Priest, E.R and Forbes, T.A.: 2001, *Magnetic Reconnection: MHD Theory and Applications*, Cambridge University Press, Cambridge, p. 180.
- Speiser, T.W.: 1965, *J. Geophys. Res.*, **70**, 4219.
- Strauss, H.R.: 1976, *Phys. Fluids*, **19**, 134.
- Wilson, H.R., et al.: 2002, *Proceedings of the 19th IAEA Fusion Energy Conference*, International Atomic Energy Agency, Vienna, in press (paper no. FT/1-5).